

Quantum optics of a Bose-Einstein condensate coupled to a quantized light field

M. G. Moore, O. Zobay, and P. Meystre
Optical Sciences Center and Department of Physics
University of Arizona, Tucson, Arizona 85721
(May 19, 1998)

We consider the interaction between a Bose-Einstein condensate and a single-mode quantized light field in the presence of a strong far off-resonant pump laser. The dynamics is characterized by an exponential instability, hence the system acts as an atom-photon parametric amplifier. Triggered by a small injected probe field, or simply by quantum noise, entangled atom-photon pairs are created which exhibit non-classical correlations similar to those seen between photons in the optical parametric amplifier. In addition, the quantum statistics of the matter and light fields depend strongly on the initial state which triggers the amplifier. Thus by preparing different initial states of the light field, one can generate matter waves in a variety of quantum states, demonstrating optical control over the quantum statistics of matter waves.

PACS numbers: 03.75.-b,42.50.-p,42.50.Ct,42.50.Dv

I. INTRODUCTION

In many ways, recently developed Bose Einstein condensates (BEC) of trapped alkali atomic vapors [1,2] are the atomic analog of the optical laser. In fact, with the addition of an output coupler, they are frequently referred to as ‘atom lasers’ [3]. Despite many interesting and important differences, the chief similarity behind the analogy is that both optical lasers and atomic BEC’s involve large numbers of identical bosons occupying a single quantum state. As a result, the physics of lasers and BEC involves stimulated processes, which due to Bose enhancement often completely dominate the spontaneous processes which play central roles in the non-degenerate regime.

Just as the discovery of the laser led to the development of nonlinear optics, so too has the advent of BEC led to remarkable experimental successes in the once theoretical field of nonlinear atom optics [4–8]. Nonlinear optics typically involves the study of multi-wave mixing, epitomized by phenomena such as parametric down conversion and phase conjugation. Due to the presence of collisions, the evolution of the atomic field is also nonlinear, and multi-wave mixing has been predicted [9–14] and observed in multi-component condensates [15], as well as in scalar condensates [16].

At the root of most optical phenomena is the dynamical interaction between optical and atomic fields. Under certain circumstances, one can formally eliminate the dynamics of the atomic field, resulting in effective interactions between light waves. Under a different set of conditions, one can eliminate the electromagnetic field dynamics, resulting in effective atom-atom interactions. These are the regimes of nonlinear optics and nonlinear atom optics, respectively. These regimes, therefore, represent limiting cases, where either the atomic or optical field is not dynamically independent, and instead follows the other field in some adiabatic manner which allows for its effective elimination.

Outside of these two regimes the atomic and optical fields are dynamically independent, and neither field is readily eliminated. In this paper we investigate the dynamics of coupled quantum degenerate atomic and optical fields in this intermediate regime. In particular, we investigate a system which is analogous to the non-degenerate optical parametric amplifier (OPA) [17,18]. However, whereas the OPA involves the creation of correlated photon pairs, this system involves the generation of correlated atom-photon pairs. The purpose of this paper is to develop a detailed theory for the interaction of quantized atomic and optical fields, with emphasis on the manipulation and control of their quantum statistics and the generation of quantum correlations and entanglement between matter and light waves.

The specific system we consider consists of a Bose-Einstein condensate driven by a strong far off-resonant pump laser which interacts with a single mode of an optical ring cavity counterpropagating with respect to the pump. The strong pump laser is treated in the usual manner as a classical, undepleted light field and furthermore it is assumed to be detuned far enough away from resonance that spontaneous emission may be safely neglected. The cavity field, henceforth referred to as the ‘probe’, is assumed to be weak relative to the pump, and is treated fully quantum mechanically as a dynamical variable. It is the dynamical interplay between this probe field and the atomic field which is the subject of interest. The pump serves as a sort of catalyst, inducing a strong atomic dipole moment, thus significantly enhancing the atom-probe interaction.

Assuming that the probe field begins in or near the vacuum state, and the atomic field consists initially of a trapped BEC, the initial dynamics is dominated by a single process: the absorption of a pump photon by a condensate atom followed by the emission of a probe photon. We remark that in the far off-resonant configuration, this is a two-photon virtual transition in which the excited atomic state population remains negligible. Due to

atomic recoil, the absorption/emission process transfers the atom from the condensate ground state to a new state that is shifted in momentum space by the two-photon recoil. This new state constitutes a second condensate component, which can be considered as a momentum side mode to the original condensate.¹ As this side mode is populated, it begins to interfere with the original condensate, resulting in fringes [21]. These fringes are seen by the pump and probe fields as a spatial density grating, which then enhances the photon scattering process.

This interplay between interference fringes and scattering can act as a positive feedback mechanism, in which case the system is unstable, and is characterized by exponential growth. Any small signal, including quantum noise, will be sufficient to trigger the instability, resulting in the generation of exponentially growing side mode and probe fields. Of course this exponential growth is eventually reversed by high intensity effects, so that the long-time dynamics is characterized by large-amplitude nonlinear oscillations.

At the present time, we focus on the small-signal regime, characterized by exponentially growing fields. In this regime, we demonstrate that the quantum state of the probe and side mode fields depends strongly on the initial conditions, so that, e.g., by injecting a small coherent light field into the probe, one can create an entirely different quantum state than that generated from the amplification of quantum vacuum fluctuations. The differences are manifested in both the quantum statistics of the individual field modes, as well as in non-classical correlations and entanglement between them.

This rest of this paper is organized as follows. Section II gives the background and relates the current theory to previous works in a variety of fields. Section III outlines the basic model for a quantized many-body atomic field interacting with a strong classical pump laser and a quantized optical cavity mode. In Sec. IV, coupled-mode equations are developed for the condensate and its momentum side modes. These equations are then linearized in Sec. V, resulting in a three-mode model which is exactly solvable. Section VI then discusses the exponential instability, with emphasis on the effects of collisions. In Sec. VII the quantum statistics of the atomic and electric

fields are investigated, and the extent to which they can be manipulated is determined. In Sec. VIII atom-photon entanglement is discussed, including an examination of two-mode squeezing between atomic and optical fields. Lastly, section IX is a discussion and conclusion, which includes estimates of the important physical parameters, as well as potential experimental obstacles.

II. BACKGROUND

The system we describe is in fact an extension into the ultracold regime of the theoretical work of Bonifacio and coworkers on the Collective Atomic Recoil Laser (CARL) [22,23]. The original CARL theory treated the atomic center-of-mass motion classically, an approximation certainly valid for hot atoms, but not sufficient to describe ultracold samples such as BEC's. Within this framework, the feedback mechanism which gives rise to the exponential instability in the CARL was outlined using a slightly different, but complementary physical picture, where the classical atomic center-of-mass motion in the optical potential of the counterpropagating pump and probe fields is responsible for the grating formation. The theory was extended to the limit of zero temperature by assuming that all of the (classical) atoms begin from rest, leading to the discovery of the so-called 'CARL cubic equation', which gives the exponential growth rate of the instability in terms of the relevant system parameters. Out of a desire to better understand the quantum statistics of the probe field, an attempt at a quantum $T = 0$ theory was made [24]. However, this attempt explicitly assumed that the wavefunctions of the individual atoms could be localized in both momentum and position space to an extent which violates the Heisenberg uncertainty principle. Thus rather than being a true quantum theory, it still treated the atoms as following 'classical' trajectories, but now with small 'quantum' fluctuations included.

Both the original classical CARL model, as well as the later 'quantum' model, fall within the ray-optics approximation for the atomic field. Clearly then, one would expect such models to break down as soon as the atomic deBroglie wavelength becomes comparable to the period of the optical potential formed by the pump and probe fields. As the wavelength of the optical potential is twice the optical wavelength, this breakdown should occur near the atomic recoil temperature, which for typical alkali atoms is on the order of microKelvins. As subrecoil temperature atomic vapors are achieved routinely through a variety of cooling techniques, a theory which properly treats the quantum motion of the atoms is required if one desires to investigate the behavior of the CARL in this regime.

With the ultimate intent of extending the CARL theory into the BEC regime, so that the unique coherence properties of condensates might be further understood and exploited by the interaction with dynamical light

¹This new state may or may not be in the same internal ground state as the original condensate, depending on the polarizations of the pump and probe photons. If the magnetic sublevels are different, then the transition would be termed a Raman transition, if the sublevels are the same, than it may be thought of as Rayleigh scattering or two-photon Bragg scattering [19,20]. As the states are already distinguished by their center-of-mass momentum states, to further distinguish them by an additional quantum number would add nothing. Our model deals specifically with the Bragg scheme, however, with only minimal modifications it could be applied to the Raman scheme as well.

fields, a quantum model of the atomic motion was formulated [25], where it was confirmed that the ray-optics versions did indeed break down for temperatures of the order of the recoil temperature or below. In fact, at $T = 0$, a second threshold for the existence of the exponential instability was discovered, occurring when the bunching process is overcome by matter-wave diffraction. For $T > T_R$, however, it was shown that the previous theories make indistinguishable predictions from the quantum theory. We remark that while in this work the atomic center of mass motion was treated quantum mechanically, the light fields were still treated classically, hence predictions concerning the quantum statistics of either the atomic or optical fields could not be made.

A full quantum model of both the atomic and optical fields was recently outlined in [26], where the subjects of manipulating quantum statistics and atom-photon entanglement were first addressed. The present paper is a detailed elaboration and extension of that work, including significant new physics. For example, utilizing the familiar s-wave scattering approach of BEC theory, the effects of atom-atom collisions are incorporated into the CARL theory for the first time. Also, in an extension of the OPA analogy, the existence of two-mode squeezing is shown to occur between a condensate side mode and the probe optical field. The current approach also differs from earlier work in that the familiar spontaneous symmetry breaking technique is no longer applied to the condensate. Instead it is assumed that a condensate well below the critical temperature is better described by a number state than a coherent state, as recent work appears to demonstrate [27,28].

The fully quantum model is similar in many ways to a system studied by Zeng and coworkers [29], in which the principle of manipulating the quantum statistics of a condensate by its interaction with a quantized light field was first proposed. This paper, however, does not recognize the existence of unstable (exponential) solutions nor the fact that the system can be triggered from quantum noise. We note that the unstable (exponential) solutions, and the possibility to initiate them from quantum vacuum fluctuations are both crucial components of this present work. Lastly, we mention the connection to recent work on matter-wave amplification by Law and Bigelow [30], which also explores the interaction between condensates and quantized light fields. In that work, however, the light field is assumed to be heavily damped, thus allowing for its dynamical elimination. As a result, only the properties of the atomic field are studied in detail.

CARL theory, including the present version, is also closely related to the theory of Recoil Induced Resonances (RIR) [31], in which the effects of atomic recoil on the pump-probe spectroscopy of an atomic vapor is investigated. This theory treats the atomic center-of-mass motion quantum mechanically. The probe field, however, is not typically treated as a dynamical variable. Hence, it does not include the effects of probe feedback, which

are necessary for exponential behavior. A detailed comparison of the RIR and CARL theories is given in [32].

III. THE BASIC MODEL

In this section we derive a fully quantized model of a gas of bosonic two-level atoms which interact with a strong, classical, undepleted pump laser and a weak, quantized optical ring cavity mode, both of which are assumed to be tuned far away from atomic resonances. As a result, single-photon transitions between atomic internal ground and excited states are highly non-resonant and the excited state population remains negligible. In this case, one can safely neglect the effects of spontaneous emission as well as the two-body dipole-dipole interaction.

We must still, however, allow for two-photon virtual transitions in the which the atomic internal state remains unchanged, but due to recoil may result in a change in the atom's center-of-mass motion. For example, an atom which absorbs a pump photon and emits a probe photon experiences a recoil kick equal to the difference of the momenta of the two photons (which for nearly counter-propagating pump and probe beams is of the order of two optical momenta). These transitions, therefore, couple different states of the atomic center-of-mass motion. Due to the quadratic dispersion relation of the atoms, these transitions will in general be non-resonant. For very cold atoms, the resultant detunings are typically on the order of the recoil frequency, i.e. much smaller than the natural linewidth of the atomic transition, γ_a , whereas the one-photon transitions which we are neglecting have a detuning many orders of magnitude larger than γ_a .

Our theory begins with the second-quantized Hamiltonian

$$\hat{\mathcal{H}} = \hat{\mathcal{H}}_{atom} + \hat{\mathcal{H}}_{probe} + \hat{\mathcal{H}}_{atom-probe} + \hat{\mathcal{H}}_{atom-pump} + \hat{\mathcal{H}}_{atom-atom}, \quad (1)$$

where $\hat{\mathcal{H}}_{atom}$ and $\hat{\mathcal{H}}_{probe}$ give the free evolution of the atomic field and the probe mode respectively, $\hat{\mathcal{H}}_{atom-probe}$ and $\hat{\mathcal{H}}_{atom-pump}$ describe the dipole coupling between the atomic field and the probe mode and pump laser, respectively, and $\hat{\mathcal{H}}_{atom-atom}$ contains the two-body s-wave scattering collisions between ground state atoms.

The free atomic Hamiltonian is given by

$$\hat{\mathcal{H}}_{atom} = \int d^3\mathbf{r} \left[\hat{\Psi}_g^\dagger(\mathbf{r}) \left(-\frac{\hbar^2}{2m} \nabla^2 + V_g(\mathbf{r}) \right) \hat{\Psi}_g(\mathbf{r}) + \hat{\Psi}_e^\dagger(\mathbf{r}) \left(-\frac{\hbar^2}{2m} \nabla^2 + \hbar\omega_a + V_e(\mathbf{r}) \right) \hat{\Psi}_e(\mathbf{r}) \right], \quad (2)$$

where m is the atomic mass, ω_a is the atomic resonance frequency, $\hat{\Psi}_e(\mathbf{r})$ and $\hat{\Psi}_g(\mathbf{r})$ are the atomic field operators for excited and ground state atoms respectively, and

$V_g(\mathbf{r})$ and $V_e(\mathbf{r})$ are their respective trap potentials. The atomic field operators obey the usual bosonic equal time commutation relations $[\hat{\Psi}_j(\mathbf{r}), \hat{\Psi}_j^\dagger(\mathbf{r}')] = \delta_{j,j'} \delta^3(\mathbf{r} - \mathbf{r}')$, and $[\hat{\Psi}_j(\mathbf{r}), \hat{\Psi}_{j'}(\mathbf{r}')] = [\hat{\Psi}_j^\dagger(\mathbf{r}), \hat{\Psi}_{j'}^\dagger(\mathbf{r}')] = 0$, where $j, j' = \{e, g\}$.

The free evolution of the probe mode is governed by the Hamiltonian

$$\hat{\mathcal{H}}_{probe} = \hbar ck \hat{A}^\dagger \hat{A}, \quad (3)$$

where c is the speed of light, k is the magnitude of the probe wave number \mathbf{k} , and \hat{A} and \hat{A}^\dagger are the probe photon annihilation and creation operators, satisfying the boson commutation relation $[\hat{A}, \hat{A}^\dagger] = 1$. The probe wavenumber \mathbf{k} must satisfy the periodic boundary condition of the ring cavity, $k = 2\pi\ell/L$, where the integer ℓ is the longitudinal mode index, and L is the length of the cavity.

The atomic and probe fields interact in the dipole approximation via the Hamiltonian

$$\begin{aligned} \hat{\mathcal{H}}_{atom-probe} &= -i\hbar g \hat{A} \int d^3\mathbf{r} \hat{\Psi}_e^\dagger(\mathbf{r}) e^{i\mathbf{k}\cdot\mathbf{r}} \hat{\Psi}_g(\mathbf{r}) \\ &+ H.c., \end{aligned} \quad (4)$$

where $g = d[ck/(2\hbar\epsilon_0 LS)]^{1/2}$ is the atom-probe coupling constant. Here d is the magnitude of the atomic dipole moment, and S is the cross-sectional area of the probe mode in the vicinity of the atomic sample (where it is assumed to be approximately constant across the length of the atomic sample).

In addition, the atoms are driven by a strong pump laser, which is treated classically and assumed to remain undepleted. The atom-pump interaction Hamiltonian is given in the dipole approximation by

$$\begin{aligned} \hat{\mathcal{H}}_{atom-pump} &= \frac{\hbar\Omega_0}{2} e^{-i\omega_0 t} \int d^3\mathbf{r} \hat{\Psi}_e^\dagger(\mathbf{r}) e^{i\mathbf{k}_0\cdot\mathbf{r}} \hat{\Psi}_g(\mathbf{r}) \\ &+ H.c., \end{aligned} \quad (5)$$

where Ω_0 is the Rabi frequency of the pump laser, related to the pump intensity I_0 by $|\Omega_0|^2 = 2d^2 I_0 / \hbar^2 \epsilon_0 c$, ω_0 is the pump frequency, and $k_0 \approx \omega_0/c$ is the pump wavenumber. The approximation indicates that we are neglecting the index of refraction inside the atomic gas, as we assume a very large detuning $\Delta = \omega_0 - \omega_a$ between the pump frequency and the atomic resonance frequency.

Finally, the collision Hamiltonian is taken to be

$$\hat{\mathcal{H}}_{atom-atom} = \frac{2\pi\hbar^2\sigma}{m} \int d^3\mathbf{r} \hat{\Psi}_g^\dagger(\mathbf{r}) \hat{\Psi}_g^\dagger(\mathbf{r}) \hat{\Psi}_g(\mathbf{r}) \hat{\Psi}_g(\mathbf{r}), \quad (6)$$

where σ is the atomic s -wave scattering length. This corresponds to the usual s -wave scattering approximation, and leads in the Hartree approximation to the standard Gross-Pitaevskii equation for the ground state wavefunction (in the absence of the driving optical fields).

We limit ourselves to the case where the pump laser is detuned far enough away from the atomic resonance

that the excited state population remains negligible, a condition which requires that $\Delta \gg \gamma_a$. In this regime the atomic polarization adiabatically follows the ground state population, allowing the formal elimination of the excited state atomic field operator. We proceed by introducing the operators $\hat{\Psi}'_e(\mathbf{r}) = \hat{\Psi}_e(\mathbf{r}) e^{i\omega_0 t}$ and $\hat{A}' = \hat{A} e^{i\omega_0 t}$, which are slowly varying relative to the optical driving frequency. The new excited state atomic field operator obeys then the Heisenberg equation of motion

$$\frac{d}{dt} \hat{\Psi}'_e(\mathbf{r}) = i\Delta \hat{\Psi}'_e(\mathbf{r}) - \left[i\frac{\Omega_0}{2} e^{i\mathbf{k}_0\cdot\mathbf{r}} + g\hat{A}' e^{i\mathbf{k}\cdot\mathbf{r}} \right] \hat{\Psi}_g(\mathbf{r}), \quad (7)$$

where we have dropped the kinetic energy and trap potential terms under the assumption that the lifetime of the excited atom, which is of the order $1/\Delta$, is so small that atomic center-of-mass motion may be safely neglected during this period. For the same reason, we are justified in neglecting collisions between excited atoms, or between excited and ground state atoms in the collision Hamiltonian (6).

We now adiabatically solve for $\hat{\Psi}'_e(\mathbf{r})$ by formally integrating Eq. (7) under the assumption that $\hat{\Psi}_g(\mathbf{r})$ varies on a time scale which is much longer than $1/\Delta$. This yields

$$\begin{aligned} \hat{\Psi}'_e(\mathbf{r}, t) &\approx \frac{1}{\Delta} \left[\frac{\Omega_0}{2} e^{i\mathbf{k}_0\cdot\mathbf{r}} - ig\hat{A}'(t) e^{i\mathbf{k}\cdot\mathbf{r}} \right] \hat{\Psi}_g(\mathbf{r}, t) \\ &- \frac{1}{\Delta} \left[\frac{\Omega_0}{2} e^{i\mathbf{k}_0\cdot\mathbf{r}} - ig\hat{A}'(0) e^{i\mathbf{k}\cdot\mathbf{r}} \right] \hat{\Psi}_g(\mathbf{r}, 0) e^{i\Delta t} \\ &+ \hat{\Psi}'_e(\mathbf{r}, 0) e^{i\Delta t}. \end{aligned} \quad (8)$$

The third term on the r.h.s. of Eq. (8) can be neglected for most considerations if we assume that there are no excited atoms at $t = 0$, so that this term acting on the initial state gives zero. The second term may also be neglected, as it is rapidly oscillating at frequency Δ , and thus its effect on the ground state field operator is negligible when compared to that of the first term, which is non-rotating.²

Dropping the unimportant terms, and then substituting Eq. (8) into the equation of motion for $\hat{\Psi}_g(\mathbf{r})$, we arrive at the effective Heisenberg equation of motion for the ground state field operator

$$\begin{aligned} \frac{d}{dt} \hat{\Psi}_g(\mathbf{r}) &= i \left[\frac{\hbar}{2m} \nabla^2 - \frac{V_g(\mathbf{r})}{\hbar} - \frac{4\pi\hbar\sigma}{m} \hat{\Psi}_g^\dagger(\mathbf{r}) \hat{\Psi}_g(\mathbf{r}) \right. \\ &\left. - \frac{g|\Omega_0|}{2|\Delta|} (\hat{a} e^{i\mathbf{K}\cdot\mathbf{r}} + \hat{a}^\dagger e^{-i\mathbf{K}\cdot\mathbf{r}}) \right] \hat{\Psi}_g(\mathbf{r}) \end{aligned}$$

²We note that in much of the literature the second and third terms are simply ignored. We choose to keep them temporarily to demonstrate that the commutation relation for $\hat{\Psi}_e(\mathbf{r})$ is preserved (to order $1/\Delta$) by the procedure of adiabatic elimination.

$$- \left(\frac{|\Omega_0|^2}{4\Delta} + \frac{g^2}{\Delta} \hat{a}^\dagger \hat{a} \right) \hat{\Psi}_g(\mathbf{r}), \quad (9)$$

where $\mathbf{K} = \mathbf{k} - \mathbf{k}_0$ is the recoil momentum kick the atom acquires from the two-photon transition, and we have introduced the new slowly-varying probe field operator $\hat{a} = -i(\Omega_0^* \Delta / |\Omega_0| |\Delta|) \hat{A}'$, which still obeys the boson commutation relation $[\hat{a}, \hat{a}^\dagger] = 1$. Here, the second to last term is simply the optical potential formed from the counterpropagating pump and probe light fields, and the last term gives the spatially independent light shift potential, which can be thought of as cross-phase modulation between the atomic and optical fields.

To complete our model, in addition to Eq. (9), we also require the equation of motion for the slowly varying probe field operator. By again substituting Eq. (8), we find that it obeys

$$\frac{d}{dt} \hat{a} = i\delta' \hat{a} - i \frac{g|\Omega_0|}{2|\Delta|} \int d^3\mathbf{r} \hat{\Psi}_g^\dagger(\mathbf{r}) e^{-i\mathbf{K}\cdot\mathbf{r}} \hat{\Psi}_g(\mathbf{r}), \quad (10)$$

where $\delta' = \omega_0 - \omega$, is the detuning between the pump and probe fields. The probe frequency is given by $\omega \approx ck$, again assuming that the index of refraction inside the condensate is negligible.

IV. COUPLED-MODE EQUATIONS

We assume that the atomic field is initially in a Bose-Einstein condensate with mean number of condensed atoms N . Furthermore, we assume that N is very large, and that the condensate temperature is small compared to the critical temperature. These assumptions allow us to neglect the noncondensed fraction of the atomic field. Thus our model does not include any effects of condensate number fluctuations.

We now introduce the atomic field operator which annihilates an atom in the condensate ground state

$$\hat{c}_0 = \int d^3\mathbf{r} \varphi_0^*(\mathbf{r}) \hat{\Psi}_g(\mathbf{r}), \quad (11)$$

where $\varphi_0(\mathbf{r}) = \langle \mathbf{r} | \varphi_0 \rangle$ satisfies the time-independent Gross-Pitaevskii equation

$$\left(\frac{\hbar}{2m} \nabla^2 - \frac{V_g(\mathbf{r})}{\hbar} - \frac{4\pi\hbar\sigma}{m} N |\varphi_0(\mathbf{r})|^2 + \frac{\mu}{\hbar} \right) \varphi_0(\mathbf{r}) = 0, \quad (12)$$

μ being the chemical potential. By differentiating Eq. (11) with respect to time, and inserting Eqs. (9) and (12) we find that the equation of motion for \hat{c}_0 is

$$\begin{aligned} \frac{d}{dt} \hat{c}_0 &= -i \left(\frac{\mu}{\hbar} + \frac{|\Omega_0|^2}{4\Delta} + \frac{g^2}{\Delta} \hat{a}^\dagger \hat{a} \right) \hat{c}_0 \\ &+ i \frac{4\pi\hbar\sigma}{m} \int d^3\mathbf{r} \varphi_0^*(\mathbf{r}) \left(N |\varphi_0(\mathbf{r})|^2 - \hat{\Psi}_g^\dagger(\mathbf{r}) \hat{\Psi}_g(\mathbf{r}) \right) \hat{\Psi}_g(\mathbf{r}) \\ &- i \frac{g|\Omega_0|}{2|\Delta|} \int d^3\mathbf{r} \varphi_0^*(\mathbf{r}) \left(\hat{a} e^{i\mathbf{K}\cdot\mathbf{r}} + \hat{a}^\dagger e^{-i\mathbf{K}\cdot\mathbf{r}} \right) \hat{\Psi}_g(\mathbf{r}). \end{aligned} \quad (13)$$

From this equation we see that the effect of the optical fields is to couple the condensate mode to two side modes, whose wavefunctions are given by

$$\langle \mathbf{r} | \varphi_\pm \rangle = \varphi_0(\mathbf{r}) e^{\pm i\mathbf{K}\cdot\mathbf{r}}. \quad (14)$$

In principle, the collision term in Eq. (13) also couples the condensate mode to various neighboring modes. However, to be consistent with the assumption of a pure condensate ($T = 0$) we assume that collisions alone do not populate any new atomic states.

Defining the field operators for the (first-order) condensate side modes as

$$\hat{c}_\pm = \int d^3\mathbf{r} \langle \varphi_\pm | \mathbf{r} \rangle \hat{\Psi}_g(\mathbf{r}), \quad (15)$$

allows us to reexpress the equation of motion for the condensate mode field operator as

$$\begin{aligned} \frac{d}{dt} \hat{c}_0 &= -i \left(\frac{\mu}{\hbar} + \frac{|\Omega_0|^2}{4\Delta} + \frac{g^2}{\Delta} \hat{a}^\dagger \hat{a} \right) \hat{c}_0 \\ &+ i \frac{4\pi\hbar\sigma}{m} \int d^3\mathbf{r} \varphi_0^*(\mathbf{r}) \left[N |\varphi_0(\mathbf{r})|^2 - \hat{\Psi}_g^\dagger(\mathbf{r}) \hat{\Psi}_g(\mathbf{r}) \right] \hat{\Psi}_g(\mathbf{r}) \\ &- i \frac{g|\Omega_0|}{2|\Delta|} (\hat{a} \hat{c}_- + \hat{a}^\dagger \hat{c}_+), \end{aligned} \quad (16)$$

where the operators \hat{c}_j obey the bosonic commutation relations

$$[\hat{c}_j, \hat{c}_{j'}^\dagger] = \langle \varphi_j | \varphi_{j'} \rangle; \quad j, j' = \{-, 0, +\}, \quad (17)$$

all other commutators being equal to zero.

We note that the three states, $|\varphi_0\rangle$, and $|\varphi_\pm\rangle$ are not mutually orthogonal, as their overlap integrals are given by

$$\begin{aligned} \langle \varphi_\mp | \varphi_\pm \rangle &= \int d^3\mathbf{r} |\varphi_0(\mathbf{r})|^2 e^{\pm i2\mathbf{K}\cdot\mathbf{r}} \\ \langle \varphi_0 | \varphi_\pm \rangle &= \int d^3\mathbf{r} |\varphi_0(\mathbf{r})|^2 e^{\pm i\mathbf{K}\cdot\mathbf{r}}. \end{aligned} \quad (18)$$

For most condensate sizes and trap configurations, however, these integrals are many orders of magnitude smaller than unity. As a result, for ‘typical’ condensates, the orthogonality approximation

$$\langle \varphi_j | \varphi_{j'} \rangle = \delta_{jj'} \quad (19)$$

yields accurate results. The range of validity of this approximation is discussed in Appendix A, where we briefly examine how the theory should be modified to properly take this non-orthogonality into account. In the following, however, we assume the validity of Eq. (19), so that the states $|\varphi_0\rangle$, and $|\varphi_\pm\rangle$ can be considered as well defined and distinct modes of the atomic field.

We now derive the Heisenberg equations for the momentum side mode field operators, found by differentiating Eq. (15) with respect to time and again inserting Eq. (9), yielding

$$\begin{aligned}
\frac{d}{dt}\hat{c}_{-,+} = & -i\left(\frac{\mu}{\hbar} + \frac{\hbar K^2}{2m} + \frac{|\Omega_0|^2}{4\Delta} + \frac{g^2}{\Delta}\hat{a}^\dagger\hat{a}\right)\hat{c}_{-,+} \\
& + i\frac{4\pi\hbar\sigma}{m}\int d^3\mathbf{r}\langle\varphi_{-,+}|\mathbf{r}\rangle\left(N|\varphi_0(\mathbf{r})|^2 - \hat{\Psi}_g^\dagger(\mathbf{r})\hat{\Psi}_g(\mathbf{r})\right)\hat{\Psi}_g(\mathbf{r}) \\
& - i\frac{g|\Omega_0|}{2|\Delta|}\left(\hat{a}^\dagger\hat{c}_{0,+2} + \hat{a}\hat{c}_{-2,0}\right) + i\frac{\hbar K k_c}{m}\hat{b}_{-,+}, \quad (20)
\end{aligned}$$

where we have introduced four new field operators $\hat{c}_{\pm 2}$ and \hat{b}_{\pm} .

The operators $\hat{c}_{\pm 2}$, which have the definitions

$$\hat{c}_{\pm 2} = \int d^3\mathbf{r}\langle\varphi_{\pm 2}|\mathbf{r}\rangle\hat{\Psi}_g(\mathbf{r}), \quad (21)$$

are the annihilation operators for the second-order side modes

$$\langle\mathbf{r}|\varphi_{\pm 2}\rangle = \varphi_0(\mathbf{r})e^{\pm i2\mathbf{K}\cdot\mathbf{r}}, \quad (22)$$

These modes will be optically coupled to third-order side modes, and so on so that a full theory of the nonlinear response of the system should include the entire manifold of side modes. In this paper, however, we focus on the linear regime, where only the first-order side modes contribute significantly.

The operators \hat{b}_{\pm} have the definitions

$$\hat{b}_{\pm} = \int d^3\mathbf{r}\langle\phi_{\pm}|\mathbf{r}\rangle\hat{\Psi}_g(\mathbf{r}), \quad (23)$$

where

$$\langle\mathbf{r}|\phi_{\pm}\rangle = (Kk_{rms})^{-1}e^{\pm i\mathbf{K}\cdot\mathbf{r}}\left(\pm i\mathbf{K}\cdot\nabla\varphi_0(\mathbf{r})\right). \quad (24)$$

Here k_c is the momentum width of the condensate state along \mathbf{K} , and is roughly given by $k_c \sim 1/W_c$, where W_c is the size of the condensate along \mathbf{K} . The factor $(Kk_c)^{-1}$ is simply a normalization coefficient.

To understand the physical meaning of the \hat{b}_{\pm} term in Eq. (20), consider what happens to a single atom after it is transferred into the state $\psi(\mathbf{r}) = \varphi_0(\mathbf{r})\exp(-i\mathbf{K}\cdot\mathbf{r})$ at time $t = 0$. Under free evolution the wavepacket of the atom, which initially has the shape of the condensate ground state, will move with group velocity $\hbar\mathbf{K}/m$ and spread at the velocity $\hbar k_c/m$. This evolution is described by the propagation equation

$$\psi(\mathbf{r}, t) = \exp[it(\hbar/2m)\nabla^2]\psi(\mathbf{r}, 0), \quad (25)$$

which for short enough times becomes

$$\begin{aligned}
\psi(\mathbf{r}, t) \approx & \left(1 - it\frac{\hbar K^2}{2m}\right)\langle\mathbf{r}|\varphi_{-}\rangle + t\frac{\hbar}{m}(\mathbf{K}\cdot\nabla\varphi_0(\mathbf{r}))e^{-i\mathbf{K}\cdot\mathbf{r}} \\
& + it\frac{\hbar}{2m}(\nabla^2\varphi_0(\mathbf{r}))e^{-i\mathbf{K}\cdot\mathbf{r}}. \quad (26)
\end{aligned}$$

The first term on the r.h.s. of Eq. (26) gives a phase shift due to the kinetic energy of the atom, the second term contributes an infinitesimal translational shift, and

the third term gives an infinitesimal amount of spreading. If we include the effects of the trap potential and collisions, this last term vanishes as all spreading effects are balanced by the trap potential for the ground state $\varphi_0(\mathbf{r})$. From Eqs. (26) and (24) we see that the state of the atom at time t can then be viewed as a coherent superposition of the state $|\varphi_{-}\rangle$ and the state $|\phi_{-}\rangle$. Thus the coupling to \hat{b}_{-} in Eq. (20) corresponds physically to translational motion of the side mode wavepacket at the recoil velocity $v_r = \hbar K/m$. Since the probability at time t that the atom is still in the ground state is simply the overlap between $\psi(\mathbf{r}, t)$ and $\psi(\mathbf{r}, 0)$, it is clear that for times $t \ll W_c/v_r$ this probability will be essentially unity, and the coupling to \hat{b}_{-} can be ignored.

V. LINEARIZED THREE-MODE MODEL

From Eq. (20), we see that the first-order side modes are optically coupled to both the condensate mode and to second-order side modes. For times short enough that the condensate is not significantly depleted, the coupling back into the condensate is subject to Bose enhancement due to the presence of $\sim N$ identical bosons in this mode. The coupling to the second-order side mode, in contrast, is not enhanced. Hence for these time scales, the higher-order side modes are not expected to play a significant role. In addition, we consider only times $t \ll W_c/v_r$, so that the translational coupling can be neglected.

These arguments suggest developing an approach where the three atomic field operators \hat{c}_0 , \hat{c}_{-} , and \hat{c}_{+} play a predominant role. Therefore, we expand the atomic field operator as

$$\hat{\Psi}_g(\mathbf{r}) = \langle\mathbf{r}|\varphi_0\rangle\hat{c}_0 + \langle\mathbf{r}|\varphi_{-}\rangle\hat{c}_{-} + \langle\mathbf{r}|\varphi_{+}\rangle\hat{c}_{+} + \hat{\psi}(\mathbf{r}), \quad (27)$$

where the field operator $\hat{\psi}(\mathbf{r})$ acts only on the orthogonal complement to the subspace spanned by the state vectors $|\varphi_0\rangle$, $|\varphi_{-}\rangle$, and $|\varphi_{+}\rangle$. As a result, $\hat{\psi}(\mathbf{r})$ commutes with the creation operators for the three central modes.

In the next step, we use Eq. (27) to expand the atomic polarization and collision terms in Eqs. (10), (16), and (20), with the eventual goal of deriving a closed set of operator equations which fully describes the system dynamics. At present, we are considering four dominant modes, the condensate and first-order side modes, as well as the optical probe mode. In the linear regime, however, we will see that the condensate mode can be dynamically eliminated, resulting in an effective three-mode model.

In expanding the polarization and collision terms by means of Eq. (27), there are two principal considerations in determining which are the dominant terms. The first is Bose enhancement, which, in the regime of negligible condensate depletion, strongly selects transitions involving the condensate mode. In order to estimate this effect, we assign a weight of \sqrt{N} for each occurrence of the operators \hat{c}_0 and \hat{c}_0^\dagger in a given term. The second consideration is momentum conservation, which comes from

the spatial integration in the polarization and collision terms. Integrals over slowly varying functions such as $|\varphi_0(\mathbf{r})|^2$, or $|\varphi_0(\mathbf{r})|^4$ are ‘momentum selected’ and dominate over integrals of rapidly oscillating functions such as $|\varphi_0(\mathbf{r})|^2 \exp(-i\mathbf{K} \cdot \mathbf{r})$.

With this approach we find that the equation of motion for the probe field operator (10) becomes

$$\frac{d}{dt}\hat{a} = i\delta'\hat{a} - i\frac{g|\Omega_0|}{2|\Delta|} [\hat{c}_-^\dagger\hat{c}_0 + \hat{c}_0^\dagger\hat{c}_+]. \quad (28)$$

Thus we see that the probe annihilation operator is coupled to the bilinear atomic field operators $\hat{c}_-^\dagger\hat{c}_0$ and $\hat{c}_0^\dagger\hat{c}_+$. These operators correspond physically to interference fringes, i.e. a periodic modulation of the atomic density, which appear because the atoms are in a coherent superposition of the side mode and condensate states. Gain in the probe can thus be interpreted as Bragg scattering of the pump due to the presence of interference fringes.

By inserting (27) into Eq. (16) we further find that the equation of motion for $\hat{c}_0^\dagger\hat{c}_0$ is given to leading order in the collision and optical terms by

$$\begin{aligned} \frac{d}{dt}\hat{c}_0^\dagger\hat{c}_0 &= i\frac{8\pi\hbar\sigma F_0}{m}\hat{c}_-^\dagger\hat{c}_0\hat{c}_+^\dagger\hat{c}_0 + i\frac{g|\Omega_0|}{2|\Delta|}\hat{a}^\dagger(\hat{c}_-^\dagger\hat{c}_0 - \hat{c}_0^\dagger\hat{c}_+) \\ &+ H.c., \end{aligned} \quad (29)$$

where

$$F_0 = \int d^3\mathbf{r}|\varphi_0(\mathbf{r})|^4. \quad (30)$$

Similarly we find that the operators $\hat{c}_-^\dagger\hat{c}_0$ and $\hat{c}_0^\dagger\hat{c}_+$ obey the equations

$$\begin{aligned} \frac{d}{dt}\hat{c}_-^\dagger\hat{c}_0 &= i\frac{\hbar K^2}{2m}\hat{c}_-^\dagger\hat{c}_0 + i\frac{4\pi\hbar\sigma F_0}{m}(\hat{c}_-^\dagger\hat{c}_0 + \hat{c}_0^\dagger\hat{c}_+)\hat{c}_0^\dagger\hat{c}_0 \\ &+ i\frac{g|\Omega_0|^2}{2|\Delta|}\hat{a}\hat{c}_0^\dagger\hat{c}_0, \end{aligned} \quad (31)$$

and

$$\begin{aligned} \frac{d}{dt}\hat{c}_0^\dagger\hat{c}_+ &= -i\frac{\hbar K^2}{2m}\hat{c}_0^\dagger\hat{c}_+ - i\frac{4\pi\hbar\sigma F_0}{m}(\hat{c}_-^\dagger\hat{c}_0 + \hat{c}_0^\dagger\hat{c}_+)\hat{c}_0^\dagger\hat{c}_0 \\ &- i\frac{g|\Omega_0|^2}{2|\Delta|}\hat{a}\hat{c}_0^\dagger\hat{c}_0. \end{aligned} \quad (32)$$

We assume that all N atoms are initially in the condensate mode, so that

$$|\psi\rangle_{t=0} = \frac{1}{\sqrt{N!}} \left(\hat{c}_0^\dagger\right)^N |0\rangle, \quad (33)$$

$|0\rangle$ being the vacuum state. We proceed by linearizing the atomic field operators around their initial expectation values, which can be determined from Eq. (33), together with the approximate commutation relations given by Eq. (19). This yields

$$\hat{c}_0^\dagger\hat{c}_0 = N(1 + \hat{\delta}_0), \quad (34)$$

$$\hat{c}_-^\dagger\hat{c}_0 = N\hat{\delta}_-, \quad (35)$$

and

$$\hat{c}_0^\dagger\hat{c}_+ = N\hat{\delta}_+, \quad (36)$$

where $\hat{\delta}_0$, $\hat{\delta}_-$ and $\hat{\delta}_+$ are therefore infinitesimal operators. In addition, we introduce a rescaled probe field operator

$$\hat{\delta}_a = \frac{\hat{a}}{\sqrt{N}}, \quad (37)$$

which, provided that the mean number of photons in the probe mode is small compared to N , is also infinitesimal. This constraint is consistent with the assumption of negligible condensate depletion.

Inserting these definitions into the equation of motion (29) for $\hat{c}_0^\dagger\hat{c}_0$, and keeping only terms linear in the infinitesimal operators, gives

$$\frac{d}{dt}\hat{\delta}_0 = 0, \quad (38)$$

which has the trivial solution $\hat{\delta}_0 = 0$. As a result, this operator can be dropped from the linearized equations for $\hat{\delta}_-$ and $\hat{\delta}_+$. This leads to a set of three coupled infinitesimal operators whose linearized equations of motion can be expressed as

$$\frac{d}{d\tau}\hat{\vec{\delta}} = i\mathbf{M}\hat{\vec{\delta}}, \quad (39)$$

where $\hat{\vec{\delta}} = (\hat{\delta}_a, \hat{\delta}_-, \hat{\delta}_+)^T$, the matrix \mathbf{M} is given by

$$\mathbf{M} = \begin{pmatrix} \delta & -\chi & -\chi \\ \chi & (1+\beta) & \beta \\ -\chi & -\beta & -(1+\beta) \end{pmatrix}, \quad (40)$$

and we have introduced the dimensionless time $\tau = \omega_r t$, $\omega_r = \hbar K^2/2m$ being the atomic recoil frequency, as well as the dimensionless control parameters

$$\chi = \frac{g|\Omega_0|\sqrt{N}}{2|\Delta|\omega_r}, \quad (41)$$

$$\delta = \delta'/\omega_r, \quad (42)$$

and

$$\beta = \frac{4\pi\hbar\sigma N F_0}{m\omega_r}. \quad (43)$$

Here χ is a dimensionless atom-probe coupling constant, δ is the pump-probe detuning in units of the atomic recoil frequency, and β gives the strength of collisions between the side modes. In Appendix B we give the effective Hamiltonian from which Eq. (39) can be derived.

The solution to Eq. (39) is then given by

$$\hat{\delta}(\tau) = e^{i\mathbf{M}\tau} \hat{\delta}(0). \quad (44)$$

From this we see that the time dependence of the infinitesimal operators is determined by the eigenvalue spectrum of the matrix \mathbf{M} . For certain values of the control parameters χ , δ , and β , one of the eigenvalues contains a negative imaginary part. When this occurs, the infinitesimal operators undergo exponential growth. This exponential instability is the focus of the next section, where we discuss its properties in detail.

VI. EXPONENTIAL INSTABILITY

The eigenvalues of \mathbf{M} are determined by the characteristic equation

$$\omega^3 - \delta\omega^2 - (1 + 2\beta)\omega + (1 + 2\beta)\delta + 2\chi^2 = 0, \quad (45)$$

which has either three real solutions, or one real and a pair of complex conjugate solutions. In the first case, the system is stable and exhibits only small oscillations around its initial state. In the second case, the system is unstable and grows exponentially, even from noise.

From Eq. (45) one finds that exponential instability occurs when

$$\chi^2 > [(3 + 6\beta + \delta^2)^{3/2} + \delta^3 - 9\delta(1 + 2\beta)]/27. \quad (46)$$

In Fig. 1 we plot the region of instability as a function of δ and χ^2 . The shaded region of Fig.1 corresponds to the instability region in the absence of collisions ($\beta = 0$). As collisions are added, the boundaries shift, illustrated by the dashed and dotted curves, which show the boundaries for the cases $\beta = .3$ and $\beta = 1.0$, respectively.

From Fig. 1, we see that for positive δ the boundary asymptotically reduces to

$$\chi^2 > 2\delta^3/27 - (1 + 2\beta)\delta/6 \quad (47)$$

i.e., the threshold value of χ^2 increases with the third power of the detuning and is only weakly influenced by the presence of collisions. On the other hand, for negative δ the asymptotic behavior is given by

$$\chi^2 > -(1 + 2\beta)\delta/2, \quad (48)$$

which only grows linearly with δ and is strongly affected by interatomic collisions, which have the effect of reducing the unstable region. In earlier work [25], it was shown that this lower threshold occurs in the absence of collisions when atomic diffraction overcomes the bunching process. For positive scattering lengths,

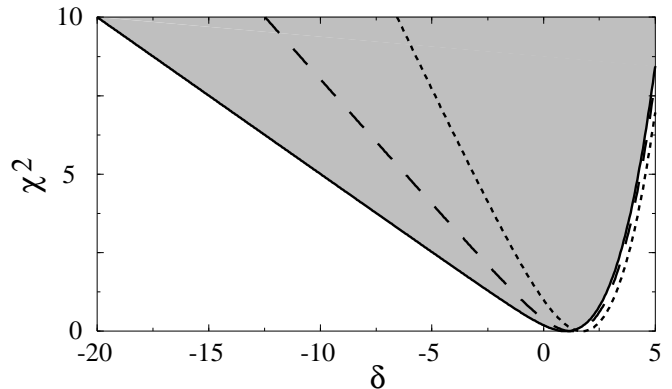


FIG. 1. Exponential instability region in the δ - χ^2 plane. The shaded area gives the unstable domain in the absence of collisions ($\beta = 0$). The dashed and dotted curves show how the boundaries change as collisions are included. They correspond to the cases $\beta = .3$ (dashed) and $\beta = 1.0$ (dotted).

we note that formation of a density grating increases the mean field energy. Collisions, therefore, should join diffraction in opposing the bunching process, resulting in a higher threshold for the instability. For negative scattering lengths, on the other hand, bunching reduces the mean field energy, hence collisions should enhance the bunching process and oppose diffraction, thus lowering the threshold. Lastly, we note that the instability region touches $\chi^2 = 0$ when $\delta = \sqrt{1 + 2\beta} \approx 1 + \beta$. This roughly corresponds to the conservation of energy in the scattering of a pump photon into the probe by an atom initially at rest.

Once we have found the eigenvectors and eigenvalues of \mathbf{M} , we can reexpress the solution (44) in the form

$$\hat{\delta}(\tau) = \mathbf{U}e^{i\Omega\tau}\mathbf{U}^{-1}\hat{\delta}(0), \quad (49)$$

where \mathbf{U} is the matrix of eigenvectors of \mathbf{M} , such that U_{ij} is the i th component of the j th eigenvector, and Ω is the diagonal matrix of eigenvalues, such that the i th diagonal element of Ω is the i th eigenvalue of \mathbf{M} . In the unstable regime, we have the eigenvalues ω_1 , $\omega_2 = \Omega + i\Gamma$, and $\omega_3 = \Omega - i\Gamma$, where ω_1 and Ω are real, and Γ is real and positive. Thus ω_1 corresponds to an oscillating solution, ω_2 an exponentially decaying solution, and ω_3 corresponds to an exponentially growing solution. Eventually, this exponentially growing solution will dominate, at which time we can neglect the other two terms, yielding the approximate solution

$$\hat{\delta}_j(\tau) = \sum_k \zeta_{jk} \hat{\delta}_k(0) e^{(\Gamma + i\Omega)\tau}, \quad (50)$$

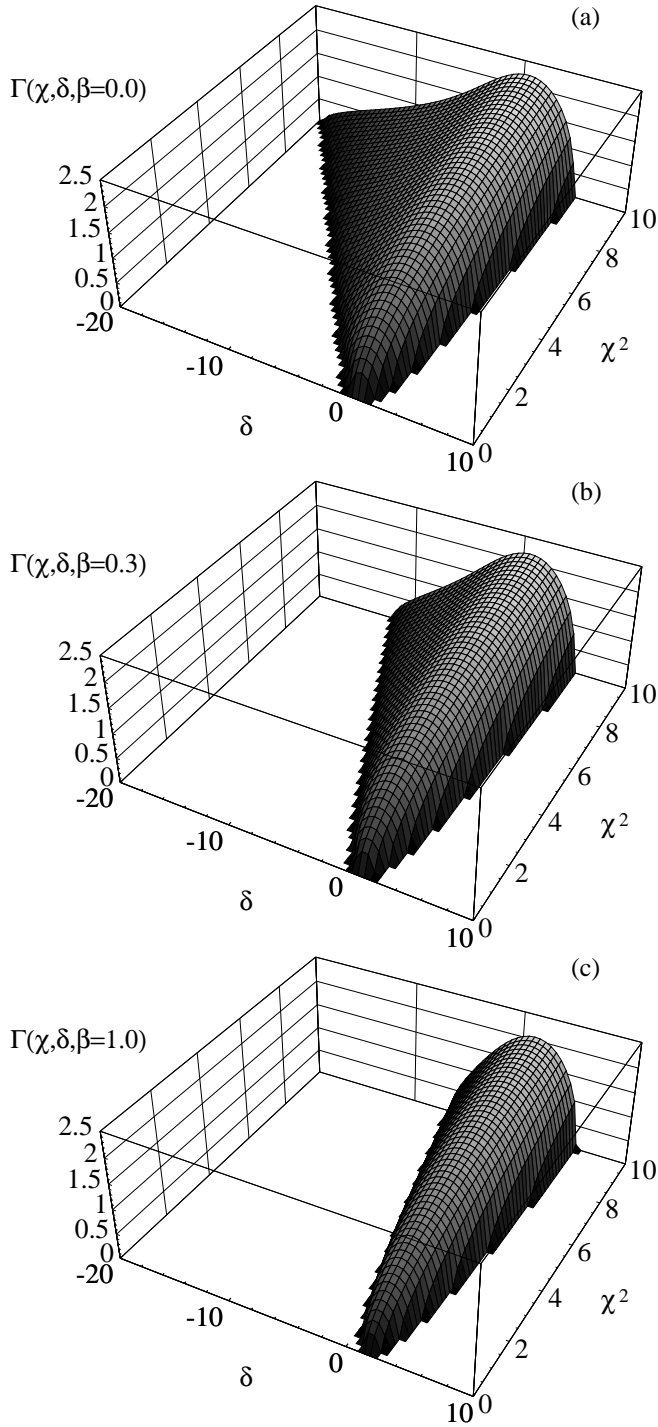


FIG. 2. Exponential growth rate Γ as a function of the scaled pump-probe detuning δ and coupling parameter χ , for various values of the collision parameter β . Figure 2a shows the case $\beta = 0$, while Figs. 2b and 2c show the cases $\beta = 0.3$ and $\beta = 1.0$, respectively.

where $\zeta_{jk} = U_{j3}U_{3k}^{-1}$. The range of validity for this approximation is roughly $1 < \Gamma\tau \ll \ln(\sqrt{N})$, where the lower limit is set by the requirement that the exponentially growing terms dominate, and the

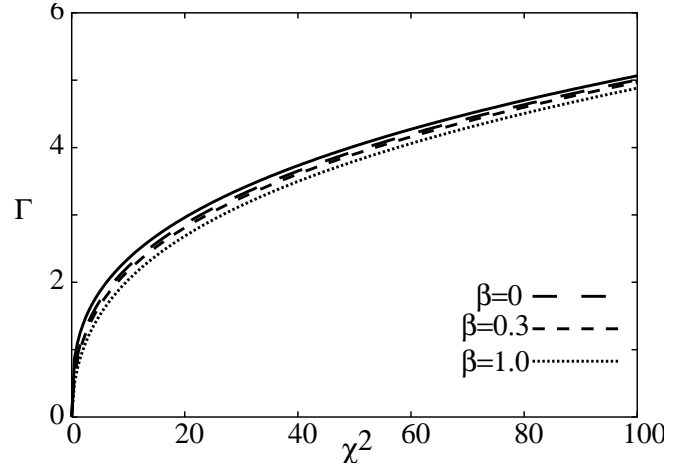


FIG. 3. The dashed lines show the growth rate Γ as a function of χ^2 for the case $\delta = 1 + \beta$, with the values of β specified in the figure. The solid line is the approximate expression given by Eq. (54).

upper limit comes from the requirement that the side mode populations remain a small fraction of the total atom number. This condition therefore formally defines the *exponential growth regime*.

The rate of exponential growth Γ has the explicit form

$$\Gamma = \frac{\sqrt{3}}{2} \left| \left[r + \sqrt{q^3 + r^2} \right]^{1/3} - \left[r - \sqrt{q^3 + r^2} \right]^{1/3} \right|, \quad (51)$$

where

$$r = -\frac{1}{3}\delta(1 + 2\beta) - \chi^2 + \frac{\delta^3}{27}, \quad (52)$$

and

$$q = -\frac{1}{9}(3 + 6\beta + \delta^2). \quad (53)$$

As this equation is complex and does not provide much insight, we have plotted Γ as a function of δ and χ^2 for three different values of β . Figure 2a shows the limit of negligible collisions $\beta = 0$, and Figs. 2b and 2c show the cases $\beta = .3$ and $\beta = 1$ respectively. From these figures, we observe that the most significant effect of collisions is to shift the lower threshold. The values of Γ in the vicinity of the maximum (for fixed χ), on the other hand, show less pronounced variations.

In cases where $\chi^2 \gg |\delta^3|, |\beta|$ we have $r \approx -\chi^2$ and $\sqrt{q^3 + r^2} \approx \chi^2$. In this case Eq. (51) reduces simply to

$$\Gamma \approx \sqrt{3}(\chi/2)^{2/3}. \quad (54)$$

Among other things, this shows that the gain scales as the number of atoms in the condensate to the 1/3 power. In Fig. 3, the growth rate Γ is plotted versus χ^2 with $\delta = 1 + \beta$, which roughly maximizes Γ for fixed χ . The three dashed curves correspond to different values of the collision parameter β , while the solid line gives the approximate result (54). This shows that the approximation is a relatively accurate estimate of the maximum gain for all values of χ^2 .

VII. QUANTUM STATISTICS

In this section we use the solution (49) to compute some of the quantum statistical properties of the system. This, however, first requires a more detailed discussion of the physical meaning of the infinitesimal operators. The first, $\hat{\delta}_a = \hat{a}/\sqrt{N}$, is clearly just a rescaling of the photon annihilation operator. From it one can compute all properties of the electric field and/or the photon statistics of the probe mode. The atomic side mode operators $\hat{\delta}_- = \hat{c}_-^\dagger \hat{c}_0/N$ and $\hat{\delta}_+ = \hat{c}_0^\dagger \hat{c}_+/N$, however, are not simply rescalings of atom annihilation operators. Rather, they are directly related to the atomic density, $\hat{\rho}(\mathbf{r}) = \hat{\Psi}_g^\dagger(\mathbf{r})\hat{\Psi}_g(\mathbf{r})$.

To illustrate this point, we expand $\hat{\rho}(\mathbf{r})$ according to Eq. (27) and linearize, yielding

$$\hat{\rho}(\mathbf{r}) = N|\varphi_0(\mathbf{r})|^2 \left[\frac{1}{2} + e^{i\mathbf{K}\cdot\mathbf{r}} (\hat{\delta}_- + \hat{\delta}_+) + H.c. \right]. \quad (55)$$

From this expression we see that the side mode operators $\hat{\delta}_\pm$ indeed describe the appearance of a density modulation with wavelength $2\pi/K$.

In addition to the atomic density, one can also express the number operators for the side modes in terms of $\hat{\delta}_\pm$. For example, we have after linearization

$$N\hat{\delta}_- \hat{\delta}_-^\dagger = \frac{\hat{c}_-^\dagger \hat{c}_0 \hat{c}_-^\dagger \hat{c}_-}{N} \rightarrow \hat{c}_-^\dagger \hat{c}_- \frac{(N+1)}{N}. \quad (56)$$

Hence with $N+1 \approx N$ the number operator for the ‘-’ side mode can be expressed as

$$\hat{c}_-^\dagger \hat{c}_- \approx N\hat{\delta}_- \hat{\delta}_-^\dagger. \quad (57)$$

Similarly the number operator for the ‘+’ side mode is given by

$$\hat{c}_+^\dagger \hat{c}_+ \approx N\hat{\delta}_+^\dagger \hat{\delta}_+. \quad (58)$$

From these number operators, one can therefore compute the number statistics of the side modes in the linear regime.

From the analytical solution (49) it is straightforward to compute the properties of the atomic and optical fields for an arbitrary initial condition. We focus on two conditions which appear readily accessible experimentally. In the first one, the probe field and the atomic side modes all begin in the vacuum state. In this case the exponential growth is triggered by vacuum fluctuations in both the probe field and the atomic density. A second possible triggering mechanism involves injecting of a weak laser field into the probe mode. Both initial situations are investigated by assuming that the probe mode is initially in the coherent state α , such that $\hat{a}|\alpha\rangle = \alpha|\alpha\rangle$, the vacuum case corresponding to $\alpha = 0$. In addition, we assume throughout that the condensate side modes begin in the vacuum state. Hence, the initial state of the

three-mode system can be expressed as $|\alpha, 0, 0\rangle$, where the first index refers to the probe mode, and the second and third indices give the states of the momentum side modes.

A. Electric field and atomic density

The expectation value of the operator $\hat{\delta}_a$ is sufficient to compute the mean electric field, and likewise, the mean values of $\hat{\delta}_-$ and $\hat{\delta}_+$ are sufficient to compute the mean atomic density. We now give analytic solutions for these physical quantities and their quantum mechanical uncertainties in the exponential growth regime, where all but the leading exponential terms can be safely neglected.

The electric field operator for the probe field is given by

$$\hat{\vec{E}}(\mathbf{r}) = \vec{\epsilon}(\mathbf{r})\mathcal{E}(\mathbf{r}, \tau)\sqrt{N}\hat{\delta}_a(\tau) + H.c., \quad (59)$$

where $\vec{\epsilon}(\mathbf{r})$ is the polarization unit vector, and

$$\mathcal{E}(\mathbf{r}, \tau) = -\sqrt{\frac{\hbar\omega}{2\epsilon_0}} \frac{\Omega_0\Delta}{|\Omega_0||\Delta|} \varphi_E(\mathbf{r}) e^{-i(\omega_0/\omega_r)\tau} \quad (60)$$

contains all constants of proportionality, the normalized spatial wavefunction of the probe mode $\varphi_E(\mathbf{r})$, and the oscillation at the pump frequency ω_0 . The mean electric field is obtained by inserting Eq. (59), and taking the quantum mechanical expectation value with respect to the initial state $|\alpha, 0, 0\rangle$, which yields

$$\vec{\epsilon}(\mathbf{r}) \cdot \langle \hat{\vec{E}}(\mathbf{r}) \rangle = \mathcal{E}(\mathbf{r}, \tau)\zeta_{aa}\alpha e^{(\Gamma+i\Omega)\tau} + c.c.. \quad (61)$$

This corresponds to an oscillating mean field with amplitude

$$E_o(\mathbf{r}) = 2|\mathcal{E}(\mathbf{r}, \tau)||\zeta_{aa}||\alpha|e^{\Gamma\tau}. \quad (62)$$

From this expression, we see that there is a nonzero mean field provided only that $\alpha \neq 0$. We also see from Eq. (61) that the mean field amplitude grows exponentially at the rate Γ , and that its frequency is shifted by $-\Omega$ away from the pump frequency. Its phase, on the other hand, has a somewhat complicated dependence on the system parameters. An analytic expression for this phase can be computed directly from Eq. (61), but as we draw no specific conclusions from it, we do not give the explicit expression here.

The variance in the electric field can also be computed in a straightforward manner from Eq. (50), yielding

$$\Delta E(\mathbf{r}) = \sqrt{2}|\mathcal{E}(\mathbf{r}, \tau)||\zeta_{a-}|e^{\Gamma\tau}. \quad (63)$$

This shows that the fluctuations also grow exponentially in time, irrespective of whether the mean field vanishes or not, and are in fact independent of α . Hence these fluctuations can be attributed solely to the amplification

of quantum noise, i.e. vacuum fluctuations in the probe electric field as well as atomic density fluctuations. While the mean field and the fluctuations both grow exponentially in time, the relative uncertainty, on the other hand, is constant in time, given by

$$\frac{\Delta E(\mathbf{r})}{E_0(\mathbf{r})} = \frac{f(\delta, \chi, \beta)}{\sqrt{2}|\alpha|}. \quad (64)$$

Here, we have introduced the fluctuation function

$$f(\delta, \chi, \beta) = \frac{|U_{3-}^{-1}|}{|U_{3a}^{-1}|}, \quad (65)$$

which can be computed directly from the eigenvectors of the matrix \mathbf{M} , and therefore depends only on the parameters χ , δ , and β . Figure 4 plots $f(\delta, \chi, \beta)$ above the δ - χ^2 plane for various values of the collision parameter β . Figure 4a shows the limit of negligible collisions ($\beta = 0$), where we see that $f(\delta, \chi, 0)$ is nearly flat in the vicinity of maximum gain ($\delta \approx 1$), where it has a value somewhere between 1 and 2. It steadily increases from this value as the pump-probe detuning δ moves in the negative direction. Figures 4b and 4c show the cases $\beta = 0.3$ and $\beta = 1.0$ respectively. From these we see that the effect of increasing the collision parameter is to flatten $f(\delta, \chi, \beta)$ as a function of χ and δ .

In a similar manner, we next calculate the mean value and variance of the atomic density. By inserting Eq. (50) into Eq. (55) and taking the expectation value with respect to the initial state, we find the expectation value of the atomic density to be

$$\langle \hat{\rho}(\mathbf{r}) \rangle = N|\varphi_0(\mathbf{r})|^2 + \rho_0(\mathbf{r}, \tau) \cos[\mathbf{K} \cdot \mathbf{r} + \Omega\tau + \phi] \quad (66)$$

where the amplitude $\rho_0(\mathbf{r})$ of the density modulation is given by

$$\rho_0(\mathbf{r}, \tau) = \sqrt{N}|\varphi_0(\mathbf{r})|^2 |\zeta_{-a} + \zeta_{+a}| |\alpha| e^{\Gamma\tau}. \quad (67)$$

Thus we see that the mean atomic density is the sum of two contributions, the initial density of the condensate plus a density modulation which grows exponentially in time, provided of course that $\alpha \neq 0$. Together with Eq. (61), this shows that the phase symmetry of the system is broken by the phase of the injected field. Only in the case $\alpha = 0$ does the symmetry remain unbroken. We note that for the atomic side modes, this is not symmetry breaking in the commonly used sense of non-zero mean fields. Rather, it is the mean atomic density modulation which acquires a nonzero phase. Note also that the mean density modulation is not stationary, as its phase is given

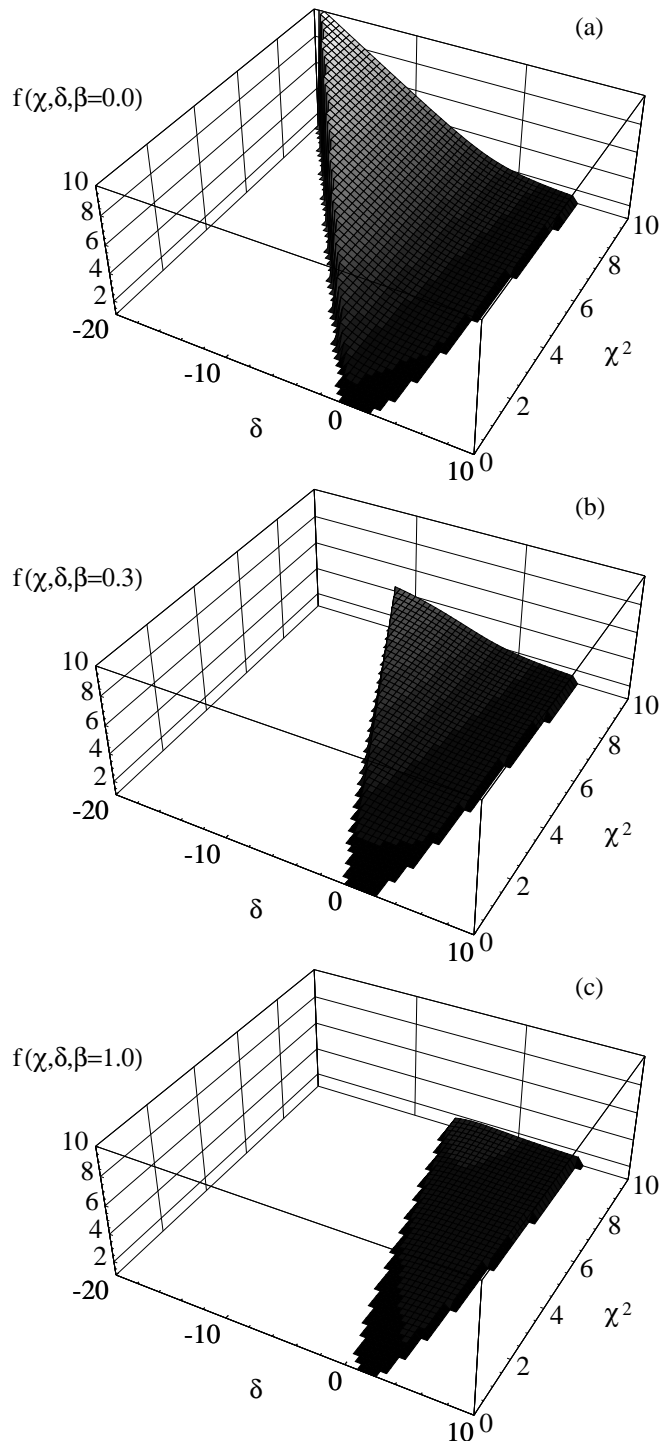


FIG. 4. Comparison of the the fluctuation function $f(\delta, \chi, \beta)$ as a function of δ and χ^2 for various values of the collision parameter β . Figure 3a gives the limit of negligible collisions ($\beta = 0$), where Figs. 3b and 3c show the cases $\beta = 0.3$ and $\beta = 1.0$, respectively.

by $\Omega\tau + \phi$, where both Ω , and ϕ are depend only on the system parameters δ , χ , and β .

The variance in the atomic density can also be readily computed in the exponential growth approximation,

yielding

$$\Delta\rho(\mathbf{r}) = 2\sqrt{N}|\varphi_0(\mathbf{r})|^2|\zeta_{--} + \zeta_{+-}|e^{\Gamma\tau}, \quad (68)$$

which shows that the density fluctuations grow exponentially in time, even in the case $\alpha = 0$. The ratio between the density variance and the modulation amplitude is constant in time, and is given by the same expression as that for the probe, i.e.,

$$\frac{\Delta\rho(\mathbf{r})}{\rho_0(\mathbf{r})} = \frac{f(\delta, \chi, \beta)}{\sqrt{2}|\alpha|}. \quad (69)$$

From Eqs. (64) and (69), we see that in the case $f(\delta, \chi, \beta) \ll |\alpha|$, both the mean electric field and the mean atomic density modulation are quantum mechanically well-defined, meaning that the quantum noise is small compared to their mean values. In this regime, both quantities could be adequately treated as classical (c-number) fields. Outside of this regime, however, the quantum fluctuations play a significant role, and a classical description no longer suffices.

The main implication of these results is that by varying the system control parameters, and in particular the injected field intensity and phase, one can vary the mean electric field and atomic density modulation continuously between two limits. For $|\alpha| \ll f(\delta, \chi, \beta)$ the fields are dominated by quantum fluctuations, and we can expect to find important non-classical effects. In the limit of a ‘strong’ injected field, however, the fluctuations are not significant, and the atomic and optical fields behave classically.

B. Intensities

We now turn to the number statistics of the three field modes, concentrating on the mean atom/photon numbers and their variances. It is convenient to reexpress the mode number operators given by Eqs. (56)-(58), as

$$\hat{N}_j = N\hat{\delta}_j^\dagger\hat{\delta}_j - \delta_{j-}, \quad (70)$$

where the index j is again the mode label a , $-$, or $+$, and the δ -function accounts for the fact that we have normally ordered the infinitesimal field operators. It is then straightforward to derive the full time-dependent solution for the mean occupation numbers $N_j \equiv \langle \hat{N}_j \rangle$ as

$$N_j = |a_{ja}(\tau)|^2|\alpha|^2 + |a_{j-}(\tau)|^2 - \delta_{j-}, \quad (71)$$

where

$$a_{ij}(\tau) = \sum_{k=1}^3 U_{ik}U_{kj}^{-1}e^{i\omega_i\tau}. \quad (72)$$

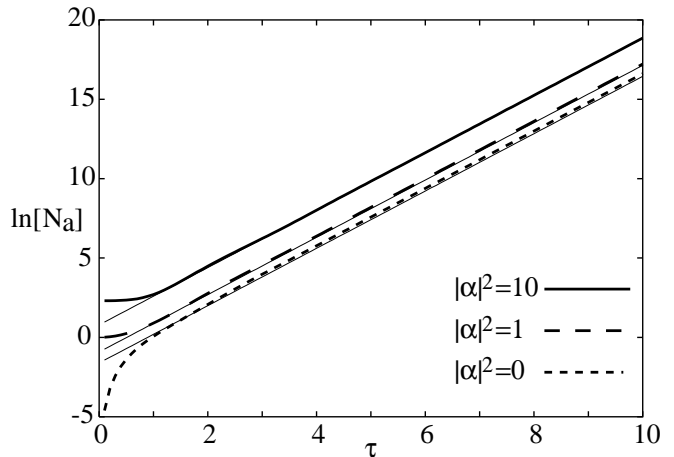


FIG. 5. Logarithmic plot of the probe intensity N_a as a function of time. This thick curves show the exact solution, given by Eq. (71), and the corresponding thin lines give the approximate solution of Eq. (75). The parameters chosen are $\delta = 1$, $\chi^2 = 1$, and $\beta = 0$. Each pair of curves corresponds to a different value of the initial probe intensity $|\alpha|^2$, as specified in the figure.

The first term in Eq. (71) can be interpreted as the stimulated contribution to the intensity,

$$[N_j]_{st} = |a_{ja}(\tau)|^2|\alpha|^2, \quad (73)$$

whereas the second term gives the spontaneous contribution,

$$[N_j]_{sp} = |a_{j-}(\tau)|^2 - \delta_{j-}, \quad (74)$$

present even in the case $\alpha = 0$. In the exponential growth regime Eq. (71) reduces to

$$N_j = (|\zeta_{ja}|^2|\alpha|^2 + |\zeta_{j-}|^2) e^{2\Gamma\tau}, \quad (75)$$

which shows that the mode occupation grows exponentially, even in the spontaneous case, where it was seen that the mean electric field and mean density modulation both vanish. The validity of the exponential approximation (75) is demonstrated in Fig. 5, where we have plotted the logarithm of the probe intensity as a function of time. The parameters chosen for the plot are $\delta = 1$, $\chi^2 = 1$, and $\beta = 0$. The thick lines give the full solution (71) for three different values of the initial probe intensity $|\alpha|^2 = 0, 1, 10$. The corresponding thin lines are the approximate solutions given by Eq. (75), which show good agreement for $\tau > 1$.

Turning now to quantum fluctuations in the occupation numbers, we find that the relative uncertainties are given by

$$\frac{\Delta N_j}{N_j} = \sqrt{1 - \frac{|a_{ja}(\tau)\alpha|^4}{N_j^2} + \frac{1}{N_j}}. \quad (76)$$

From Eq. (71) it is clear that the second term under the radicand in the above expression is ≤ 1 ,

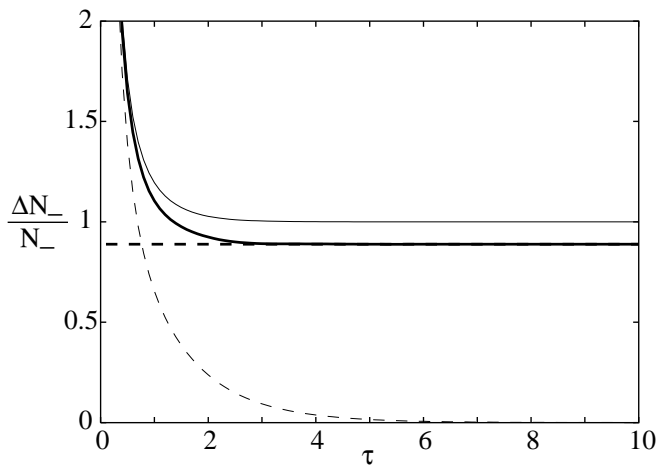


FIG. 6. The side mode number variance $\Delta N_-/N_-$ is plotted versus time (thick solid line). Also shown are the approximate solution given by Eq. (77) (thick dashed line) as well as the variances for a thermal state (thin solid line) and a coherent state (thin dashed line) with the same mean value N_- . The parameters chosen are $\delta = 1$, $\chi^2 = 1$, $\beta = 0$, and $\alpha = 1$.

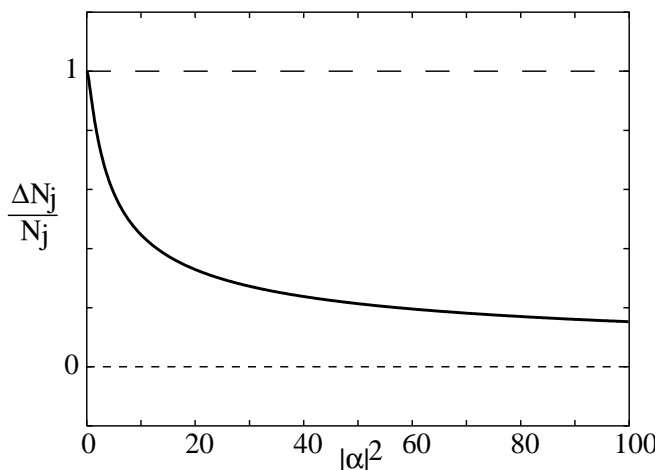


FIG. 7. The long time limit of $\Delta N_j/N_j$ is plotted against the initial probe intensity $|\alpha|^2$ (thick solid line). It varies continuously between thermal (upper dashed line) and coherent (lower dashed line) limits. The parameters chosen are $\Delta = 1$, $\chi^2 = 1$, and $\beta = 0$.

which means that as a function of time, the relative uncertainty is always between $\sqrt{1/N}$, characteristic of the fluctuations found in a coherent state, and $\sqrt{1 + 1/N}$, which is the signature of thermal number fluctuations.

While for very short times the relative uncertainty may fluctuate between the thermal and coherent limits, once the exponentially growing terms dominate, the relative uncertainty eventually reaches a steady-state value given by

$$\frac{\Delta N_j}{N_j} = \sqrt{1 - \frac{|\alpha|^4}{[|\alpha|^2 + f^2(\chi, \delta, \beta)]^2}}. \quad (77)$$

Thus we see that when $|\alpha|^2 \gg f^2(\chi, \delta, \beta)$, the relative uncertainty tends towards zero, while in the opposite case, it tends toward one. These limits can be labeled as the stimulated and spontaneous limits respectively. In the intermediate regime, the fluctuations can be varied continuously between the thermal and coherent limits, e.g. by varying the injected laser intensity, thus achieving optical control over the quantum statistics of matter waves.

The behavior of the particle number variances is illustrated by Figs. 6 and 7. In Fig. 6 the full time dependence of $\Delta N_-/N_-$ is shown (thick solid line). Also shown are the approximate solution given by Eq. (77) (thick dashed line) as well as the variances for a thermal state (thin solid line) and a coherent state (thin dashed line) with the same mean value N_- . The parameters chosen are $\delta = 1$, $\chi^2 = 1$, $\beta = 0$, and $\alpha = 1$. Thus we see that the variance always falls between those of thermal and coherent fields. We also see that the long time behavior is well approximated by Eq. (77). In Fig. 7 the steady state value for large τ is plotted as a function of the initial probe intensity $|\alpha|^2$. Thus we see that it is possible to vary the output continuously over the whole range between thermal and coherent limits, simply by varying the initial probe intensity. The parameters chosen for the figure are $\delta = 1$, $\chi^2 = 1$, and $\beta = 0$.

VIII. ATOM-PHOTON ENTANGLEMENT

We have previously discussed the analogy between the present system and the non-degenerate optical parametric amplifier (OPA). One of the most interesting applications of the OPA is the generation of entangled quantum optical states. We show that similar entanglements occur in the present system, but they are now between atomic and optical field modes. We first examine the two-mode intensity correlation functions, which give a measure of entanglement, and can be used to determine whether or not non-classical correlations exist between the three field modes. We then discuss the issue of two-mode squeezing, and show how this phenomenon manifests itself in the present system.

A. Two-mode intensity correlations

The equal-time intensity correlation functions are defined in the usual manner as

$$g_{ij}^{(2)} = \frac{\langle \hat{N}_i \hat{N}_j \rangle - \delta_{ij} \langle \hat{N}_j \rangle}{\langle \hat{N}_i \rangle \langle \hat{N}_j \rangle}. \quad (78)$$

For classical fields, the two-mode ($i \neq j$) correlations are constrained by the Cauchy-Schwartz inequality

$$g_{ij}^{(2)} \leq [g_{ii}^{(2)}]^{1/2} [g_{jj}^{(2)}]^{1/2}. \quad (79)$$

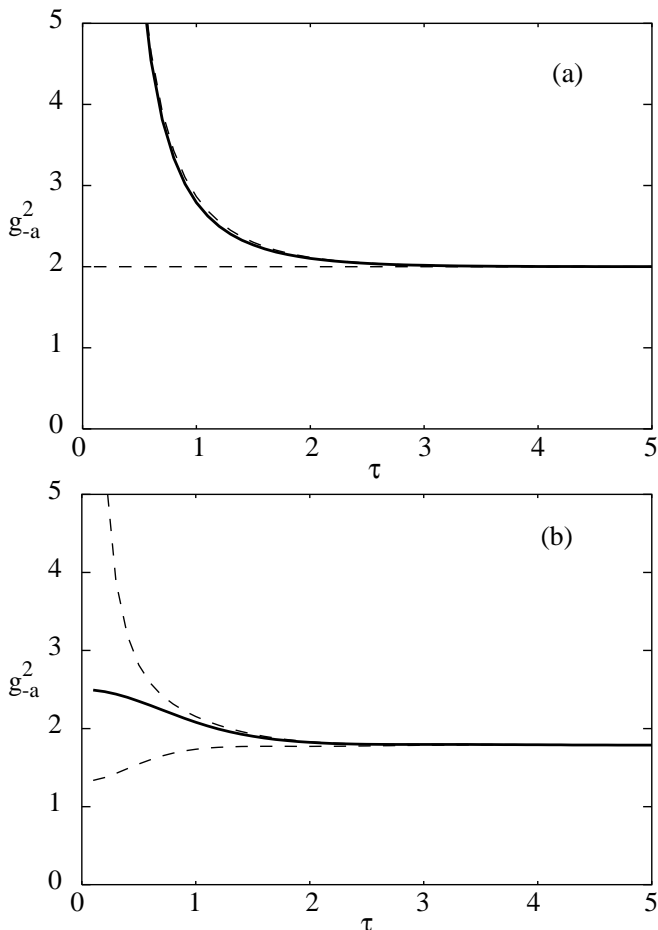


FIG. 8. The cross-correlation function $g_{-a}^{(2)}$ is plotted as a function of time (solid line). The upper dashed line gives the maximum allowed by quantum mechanics, while the lower dashed line gives the upper limit for classical correlations only. The parameters chosen are $\delta = 1$, $\chi^2 = 1$, and $\beta = 0$. Figure 8a corresponds to triggering from noise ($\alpha = 0$), while Fig. 8b shows the case $\alpha = 1$.

Quantum mechanical fields, however, can violate this inequality and are instead constrained by

$$g_{ij}^{(2)} \leq \left[g_{ii}^{(2)} + \frac{1}{\langle \hat{N}_i \rangle} \right]^{1/2} \left[g_{jj}^{(2)} + \frac{1}{\langle \hat{N}_j \rangle} \right]^{1/2}, \quad (80)$$

which reduces to the classical result in the limit of large intensities.

We focus our attention on the spontaneous case $\alpha = 0$. Here the single-mode intensity correlation functions are those of thermal fields, $g_i^{(2)}(\tau) = 2$. In this case, the equal-time intensity cross-correlation functions are found to be

$$g_{a-}^{(2)} = g_{-+}^{(2)} = \left[2 + \frac{1}{N_a + N_+} \right]^{1/2} \left[2 + \frac{1}{N_-} \right]^{1/2},$$

$$g_{a+}^{(2)} = 2. \quad (81)$$

From Eq. (81) we see that both $g_{a-}^{(2)}(\tau)$ and $g_{-+}^{(2)}(\tau)$ violate the Cauchy-Schwartz inequality, while $g_{a+}^{(2)}(\tau)$ is consistent with classical cross-correlations. Furthermore, the explicit evaluation of the ζ_{ij} 's shows that $I_+(\tau) \ll I_a(\tau)$, which implies that $g_{a-}^{(2)}(\tau)$ is very close to the maximum violation of the classical inequality consistent with quantum mechanics, whereas for $g_{-+}^{(2)}(\tau)$ the violation is not close to the allowed maximum. In the two-mode parametric amplifier, the two-mode correlation function shows the maximum violation of the Cauchy-Schwartz inequality consistent with quantum mechanics. In the three-mode system, however, the two-mode cross-correlation functions involve a trace over the third mode, hence it is not surprising that they are not maximized. This is illustrated in Fig. 8a, where we have plotted the correlation function $g_{-a}^{(2)}$ as a function of time (solid line). Also shown for comparison are the quantum mechanical upper limit given by Eq. (80) (upper dashed line), as well as the classical upper limit given by Eq. (79) (lower dashed line). The parameters are $\delta = 1$, $\chi^2 = 1$, $\beta = 0$, and $\alpha = 0$. We see that when the system is triggered by vacuum fluctuations alone, $g_{-a}^{(2)}$ is virtually indistinguishable from the maximum allowed by quantum mechanics.

If we now allow for an injected coherent probe field ($\alpha \neq 0$), we first note that the intensities are increased by approximately $|\alpha|^2$, which means that the time scale on which the classical and quantum upper limits (79) and (80) converge is reduced by $1/|\alpha|^2$, making an experimental confirmation of quantum correlations more difficult. In addition, whereas for the spontaneous case $\alpha = 0$, numerics show the cross-correlation $g_{a-}^{(2)}$ follows almost exactly the quantum upper limit (80) for all $t > 0$, for $\alpha \neq 0$, it lies somewhere in between the quantum (80) and classical (79) limits. As α is increased, it falls ever closer to the classical upper limit, so that in the limit of very large α , the fields exhibit classical cross-correlations only. This effect is illustrated by Fig. 8b, which is identical to 8a, except that now we have taken $\alpha = 1$. This shows that even when the probe field initially contains only one photon on average, it is enough to significantly reduce the quantum correlations from the quantum mechanical maximum.

B. Two-mode squeezing

To complete the study of atom-photon entanglement we complement the investigation of intensity cross-correlations with a discussion of phase-sensitive two-mode correlations. Drawing again on the similarity between the current model and the two-mode parametric amplifier we expect the correlations between the cavity mode and the atomic side-mode “-” to be of particular interest as a “squeezing-like” behavior may occur. In analogy to the parametric amplifier we thus introduce the quadrature components of the superposed atomic and op-

tical fields

$$X_\theta = \sqrt{\frac{N}{2}}(\hat{\delta}_a e^{i\theta} + \hat{\delta}_- e^{-i\theta} + h.c.). \quad (82)$$

The variance of X_θ is given by

$$\begin{aligned} V(X_\theta) &= \langle X_\theta^2 \rangle - \langle X_\theta \rangle^2 \\ &= |a_{a-}(\tau)e^{i\theta} + a_{--}(\tau)e^{-i\theta}|^2. \end{aligned} \quad (83)$$

Note that this variance (83) is independent of the injected signal strength α , just as with the electric field, atomic density, and mode intensities. It follows from Eq. (83) that the angle $\theta_{min}(\tau)$ that minimizes the quadrature variance is determined by

$$\arg[a_{a-}(\tau)a_{--}^*(\tau)] + 2\theta_{min}(\tau) = \pi \quad (84)$$

so that the corresponding minimum of V for fixed τ is given by

$$V_{min}(\tau) = [|a_{a-}(\tau)| - |a_{--}(\tau)|]^2 \quad (85)$$

The Heisenberg uncertainty principle gives $V(X_\theta)V(X_{\theta+\pi/2}) \geq 1$, hence, a quadrature component is squeezed provided $V(X_\theta) < 1$.

In Fig. 9, we display $V_{min}(\tau)$ for various values of the system parameters. We find that for $\delta \approx 1$, i.e., maximum exponential growth rate, V_{min} is a concave function of τ displaying a single (global) minimum which is typically of the order of 10^{-1} (cf. the full and dashed curves). The maximum squeezing time τ_m , i.e., the largest τ for which $V_{min}(\tau) = 1$, is given by $\tau_m = 3.5$ for $\chi = 1$, $\delta = 1$, and $\beta = 0$ whereas for $\chi = 10$ τ_m decreases to a value of 0.20. The reduction is due to the increase in the exponential growth rate Γ with larger χ . From Fig. 9, we see that squeezing does indeed occur over a broad range of parameters, however it only persists over intermediate time scales. For long times, $V_{min}(\tau)$ is dominated by the exponential behavior, which eventually leads to the violation of the squeezing condition. This is in contrast to the two-mode OPA, where the quadrature component remains squeezed for all time.

To understand how the presence of a third mode quenches the squeezing, we reexpress the squeezing condition with the help of Eq. (74), yielding

$$([N_a]_{sp} - [N_-]_{sp})^2 < 2[N_a]_{sp}. \quad (86)$$

As our analysis of squeezing so far has not made explicit use of the particular form of the matrix \mathbf{M} , it can also be applied to the standard two-mode optical parametric amplifier. One simply chooses a suitable \mathbf{M} where the third mode is decoupled.

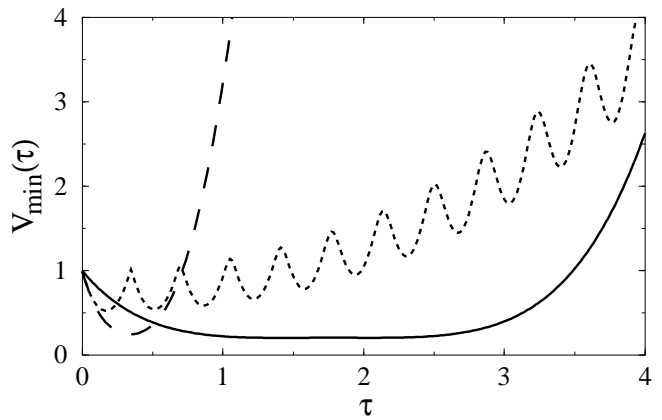


FIG. 9. Minimum variance V_{min} of the quadrature components X_θ as a function of τ for parameter values $\chi = 1.0$, $\delta = 1.0$, $\beta = 0.0$ (full curve); $\chi = 3.0$, $\delta = 1.0$, $\beta = 0.0$ (dashed); $\chi = 3.0$, $\delta = -17.0$, $\beta = 0.0$ (dotted).

In this case, the solution is well known [18], and the two modes are symmetrical, with equal populations. This means that the l.h.s. of Eq. (86) is always zero, and the squeezing condition is satisfied for all times. However, once the third mode is included, it introduces a small imbalance between the populations of the two original modes, since momentum conservation requires that $N_a + N_+ = N_-$. On long time scales, the l.h.s. of Eq. (86) grows like $\exp(i4\Gamma\tau)$, whereas the r.h.s. only grows as $\exp(i2\Gamma\tau)$. Therefore, the squeezing condition (86) must eventually cease to be satisfied.

The introduction of moderate collisional interactions, i.e., $g < 1$, only leads to quantitative modifications of V_{min} without altering the characteristic features. An interesting change in behavior occurs, however, if δ is tuned closer to the borders of the amplification range (dotted curve in Fig. 6). Under these circumstances squeezing still occurs but V_{min} displays an oscillating behavior as a function of τ . These oscillations are caused in part by the reduction of the exponential growth rate and a simultaneous increase of the imaginary part of the eigenvalues of the matrix \mathbf{M} .

The extremal angle θ_{min} varies as time evolves, eventually attaining a constant value when the behavior of $V_{min}(\tau)$ is dominated by exponential growth. However, in many cases $V(X_\theta)$ is well approximated by $V_{min}(\tau)$ if θ is chosen in the vicinity of $\theta_{min}(\tau)$.

IX. DISCUSSION AND CONCLUSION

The fundamental time scale in the system is the inverse growth rate Γ^{-1} . It is estimated by Eq. (54) in units of the inverse recoil frequency ω_r^{-1} which, for sodium is given by $\omega_r \approx 1.7 \mu\text{s}$. The estimated growth rate is then of the order of $\chi^{2/3} = (\sqrt{2n_e N} g / \omega_r)^{2/3}$, where $n_e = (I_0 / 8I_{sat})(\gamma / \Delta)^2$. Here I_0 is the pump intensity, I_{sat} the atomic saturation intensity, and γ the

atomic spontaneous decay rate. For sodium atoms we have $I_{sat} = 6.33\text{mW/cm}^2$. The parameter n_e equals the fraction of excited atoms, hence, under the far-off resonance conditions we are considering, we have $n_e \ll 1$. If we chose the ring cavity length $L = 0.1\text{m}$ and effective cross section $S = 10^{-9}\text{m}^2$, the atom-cavity coupling constant g is of the order 10^6 s^{-1} so that $g/\omega_r \approx 1$. As one has a great latitude in choosing the values of n_e and the total number N of atoms in the BEC it should be possible to vary the exponential growth rate over a wide range.

Our choice of n and n_e is constrained, however, by the requirement that the spontaneous heating rate \mathcal{L} be much smaller than the exponential growth rate Γ , so that spontaneous emission can in fact be neglected. The heating rate (in units of ω_r) is given by $\mathcal{L} = n_e\gamma/\omega_r$. As $\gamma/\omega_r \approx 10$ the condition $\Gamma \gg \mathcal{L}$ translates into $N \gg 10^3 n_e^2$. As $n_e \ll 1$, this condition is practically always fulfilled. Also related to spontaneous emission is the two-body dipole-dipole interaction, which acts in addition to ground-state collisions. For very cold atoms whose de Broglie wave length is large in comparison to the pump laser wavelength the dipole-dipole interaction can be approximated as a contact interaction [33]. Comparing the strength of this interaction to that ground-state collisions one finds that the former is negligible under the condition $n_e \ll 8\hbar k_0^3\sigma/m\gamma$, which translates to $n_e \ll 10^{-3}$ for sodium atoms. If this condition is not met the dipole-dipole interaction can still be accounted for to a good degree of approximation by modifying the scattering length according to $\sigma \rightarrow \sigma - I_0\gamma^3/32I_{sat}\Delta^2\omega_r$.

Another important parameter is the collision parameter β . Estimating the quantity NF_0 to be of the order of the atomic density we find the collision parameter β to lie in the range 0.1–1 for 'typical' densities around 10^{15} cm^{-3} . If β could be measured by, e.g. observing the boundaries of the instability regime, than this could be used as a novel means to determine the atomic s-wave scattering length.

In a realistic optical cavity, the lifetime of a photon is of the order of 1-10ns, corresponding to a decay rate of 10^3 to 10^4 in units of the recoil frequency. This tells us how large the growth rate Γ would have to be to result in a buildup of photons in the cavity. Since Γ goes like $N^{1/3}$ we would likely need a very large condensate, with 10^{12} or more atoms, to achieve this. In the future, larger condensates and better cavities, will be available, at which point the theory could presumably be tested. Future research will study the quantum statistics of the system under the influence of probe field damping, which will relate the model more closely to current experiments. For example, recent experiments by W. Ketterle's group involving a condensate driven by a far-off resonant pump laser have demonstrated the appearance of distinct momentum side modes as a consequence of spontaneous emission. While these experiments involve at most one spontaneous photon at a time in the condensate, they clearly demonstrate many aspects of the theory we have described, as

well as the importance of continuing to develop a nonlinear/quantum optics approach to the theory of optically driven Bose-Einstein condensates.

ACKNOWLEDGMENTS

This work is supported in part by the U.S. Office of Naval Research Contract No. 14-91-J1205, by the National Science Foundation Grant PHY98-01099, by the U.S. Army Research Office and by the Joint Services Optics Program.

APPENDIX A: NON-ORTHOGONALITY

By properly taking into account the non-orthogonality of the atomic field modes, it can be shown that the only surviving effect in the linearized theory is the modification of the atomic polarization term in the equation of motion for the probe field (10) to include a second scattering mechanism in which a condensate scatters a photon without changing its center of mass state. As a consequence of momentum conservation, this process is suppressed by a factor $\langle\varphi_0|\varphi_-\rangle$ relative to the process which transfers the atom to the side mode state. Bose enhancement, on the other hand, is stronger for this transition by a factor \sqrt{N} , because we now have N identical bosons in both the initial and final states. Thus it is the product $\sqrt{N}\langle\varphi_0|\varphi_-\rangle$ which must be negligible if we are to make the orthogonality approximation.

More precisely, we find that the quantum statistics must be modified by taking $\alpha \rightarrow \alpha - s$, where

$$s = \frac{\chi\varphi_0|\varphi_-\rangle\sqrt{N}}{(\Omega - i\Gamma)}, \quad (87)$$

in order to account for this additional scattering mechanism. Thus when α is comparable to $f(\delta, \chi, \beta)$, the condition $|s| \ll |\alpha|$ allows us to neglect s . For the case $\alpha \ll f(\delta, \chi, \beta)$, on the other hand, requires $|s| \ll f(\delta, \chi, \beta)$. Since $f(\delta, \chi, \beta)$ is typically of order 1, then the condition $|s| \ll 1$ is sufficient to satisfy both conditions.

For a dilute condensate, the ground state wave function $\varphi_0(\mathbf{r})$ is given to a approximately by the single-particle ground state. For a harmonic trap with \mathbf{K} taken along the z -axis, one has thus

$$\langle\varphi_0|\varphi_-\rangle = e^{-\frac{1}{4}(KW_c)^2}, \quad (88)$$

where K approximately twice the optical wave number, and W_c is the condensate width along \mathbf{K} . For a dilute condensate which is an order of magnitude or larger than the optical wavelength, this integral is clearly vanishingly small, and $s \approx 0$ for all reasonable values N and the system parameters δ , χ , and β .

In the case of a dense condensate the density distribution can be described with the help of the Thomas-Fermi approximation, i.e.,

$$|\phi_0(\mathbf{r})|^2 = [\mu - V_g(\mathbf{r})]m/(4\pi\hbar^2\sigma N), \quad (89)$$

where the chemical potential μ is determined from the normalization requirement. Starting from Eq. (89) and choosing the recoil wave vector \mathbf{K} to lie parallel the z -axis, the overlap integral is found to be

$$\langle\varphi_0|\varphi_-\rangle = 15j_2(KW_c)/(KW_c), \quad (90)$$

where j_2 is the modified Bessel function, and the W is the condensate width along \mathbf{K} . For condensates which are large compared to the optical wavelength, Eq. (90) behaves like $-15\sin(KW_c)/(KW_c)^3$. So assuming that $KW_c = 100$, which corresponds to a $10\mu\text{m}$ condensate, we would need $\chi\sqrt{N}/(\Omega - i\Gamma)$ to be of the order 10^6 in order to achieve an appreciable value of s , and this is much larger than is currently feasible. However, if, for example, \mathbf{K} is oriented parallel to a trap axis with tight confinement KW_c need not be too large and diffraction effects may be appreciable.

A more efficient way to increase s consists in confining the condensate in three-dimensional rectangular trap potential. In this case the Thomas-Fermi approximation gives $|\varphi_0(\mathbf{r})|^2 = 1/V$, V being the volume of the trap. With \mathbf{K} chosen along the z -axis of the trap, and W_c being the width of the box in this direction, one obtains for the overlap integral

$$\langle\varphi_0|\varphi_-\rangle = e^{-iKW_c/2} \frac{\sin(KW_c/2)}{KW_c/2}. \quad (91)$$

For large KW_c I now decays only as $(KW_c)^{-1}$.

APPENDIX B: EFFECTIVE HAMILTONIAN

If we define $\hat{C}_- = \sqrt{N}\delta_-^\dagger$, and $\hat{C}_+ = \sqrt{N}\delta_+$, then these operators obey approximately bosonic commutation relations, and the system of equations (39) can be derived from the effective Hamiltonian

$$\begin{aligned} \mathcal{H}_{eff} = & (1 + \beta)\hat{C}_-^\dagger\hat{C}_- + (1 + \beta)\hat{C}_+^\dagger\hat{C}_+ - \hat{a}^\dagger\hat{a} \\ & + \beta(\hat{C}_-^\dagger\hat{C}_+^\dagger + \hat{C}_-\hat{C}_+) \\ & + \chi(\hat{a}^\dagger\hat{C}_-^\dagger + \hat{a}\hat{C}_- + \hat{a}^\dagger\hat{C}_+ + \hat{a}\hat{C}_+^\dagger). \end{aligned} \quad (92)$$

-
- [1] M. H. Anderson, J. R. Ensher, M. R. Matthews, and E. A. Cornell, *Science* **269**, 198 (1995).
[2] K. B. Davis, M. O. Mewes, M. R. Andrews, N. J. van Druten, D. S. Durfee, D. M. Kurn, and W. Ketterle, *Phys. Rev. Lett.* **75**, 3969 (1995).
[3] M. O. Mewes, M. R. Andrews, D. M. Kurn, D. S. Durfee, C. G. Townsend, and W. Ketterle, *Phys. Rev. Lett.* **78**, 582 (1997).

- [4] G. Lenz, P. Meystre, and E. M. Wright, *Phys. Rev. Lett.* **71**, 3271 (1993).
[5] G. Lenz, P. Meystre, and E. M. Wright, *Phys. Rev. A* **50**, 1681 (1994).
[6] Weiping Zhang, D. F. Walls, and B. C. Sanders, *Phys. Rev. Lett.* **71**, 60 (1994).
[7] Weiping Zhang and D. F. Walls, *Phys. Rev. A* **49**, 3799 (1994).
[8] Y. Castin and K. Mølmer, *Phys. Rev. A* **51**, 3426 (1995).
[9] E. Goldstein, K. Plättner, and P. Meystre, *Quant. Semi-class. Opt.* **7**, 743 (1995).
[10] E. Goldstein, K. Plättner, and P. Meystre, *J. Res. Nat. Inst. Stand. Technol.* **101**, 583 (1996).
[11] M. Trippenbach, Y. Band, and P. S. Julienne, *Optics Express* **3**, 530 (1998).
[12] C. K. Law, H. Pu, and N. P. Bigelow, *Phys. Rev. Lett.* **81**, 5257 (1998).
[13] E. V. Goldstein and P. Meystre, *Phys. Rev. A* **59**, 1509 (1999).
[14] E. Goldstein and P. Meystre, *Phys. Rev. A* **58**, in press (1999).
[15] J. Stenger, S. Inouye, D. M. Stamper-Kurn, H. J. Meisner, A. P. Chikkatur, and W. Ketterle, *Nature* **396**, 345 (1998).
[16] W. D. Phillips, private communication.
[17] Y. R. Shen, *The Principles of Nonlinear Optics* (John Wiley & Sons, New York, 1984) and references therein.
[18] D. F. Walls and G. J. Milburn, *Quantum Optics* (Springer-Verlag, Berlin, 1994).
[19] M. Kozuma, L. Deng, E. W. Hagley, J. Wen, R. Lutwak, K. Helmerson, S. L. Rolston, and W. D. Phillips, *Phys. Rev. Lett.* **82**, 871 (1999).
[20] J. Stenger, S. Inouye, A. P. Chikkatur, D. M. Stamper-Kurn, D. E. Pritchard, and W. Ketterle, LANL eprint, cond-mat/9901109.
[21] M. R. Andrews, C. G. Townsend, H. J. Miesner, D. S. Durfee, D. M. Kurn, and W. Ketterle, *Science* **275**, 637 (1997).
[22] R. Bonifacio and L. De Salvo, *Nucl. Instrum. Methods Phys. Res. A* **341**, 360 (1994).
[23] R. Bonifacio, L. De Salvo, L. M. Narducci, and E. J. D'Angelo, *Phys. Rev. A* **50**, 1716 (1994).
[24] R. Bonifacio, *Optics Comm.* **146**, 236 (1998).
[25] M. G. Moore and P. Meystre, *Phys. Rev. A* **58**, 3248 (1998).
[26] M. G. Moore and P. Meystre, *Phys. Rev. A* **59**, in press (1999).
[27] M. Wilkens and C. Weiss, *J. of Mod. Opt.* **44**, 1801 (1997).
[28] S. Grossmann and M. Holthaus, *Phys. Rev. Lett.* **79**, 3557 (1997).
[29] H. Zeng, F. Lin, and Weiping Zhang, *Phys. Lett. A* **201**, 397 (1995).
[30] C. K. Law and N. P. Bigelow, *Phys. Rev. A* **58**, 4791 (1998).
[31] J. Guo, P. R. Berman, B. Dubetsky, and G. Grynberg, *Phys. Rev. A* **46**, 1426 (1992).
[32] P. R. Berman, *Phys. Rev. A* **59**, 585 (1999).
[33] M. Holzmann and J. Audretsch, *Europhys. Lett.* **40**, 31 (1997).

[34] W. Ketterle, private communication.